Supporting Information

Halevy 10.1073/pnas.1213148110

SI Materials and Methods

Model Geometry and Transport. Schematic model geometry is shown in Fig. 1 of the main text. The box volumes and surface areas (where applicable) are in Table S1. Water exchange fluxes among the boxes and references for these values are in Table S2. The main seawater boxes (shallow, intermediate, deep, downwelling high-latitude, and upwelling high-latitude) and the exchange of water among them are similar to a published five-box ocean model, which captures the behavior of the ocean during ocean-anoxic events (1). Of the five main boxes, a sediment box underlies only the deep ocean box. Additional seawater boxes represent environments in which the chemical properties of the water column may get preserved in the underlying sediments (continental shelves, estuaries, upwelling zones, near-hydrothermal seafloor). Accordingly, sediment boxes underlie these additional boxes.

Exchange between the global continental shelf and the surface and intermediate ocean boxes was estimated by scaling up exchange estimates between the European shelf and the open ocean (2). Exchange between the intermediate and upwelling boxes was estimated and is uncertain. However, the value of this exchange flux does not affect the results of the model other than to distinguish between the intermediate and upwelling boxes. At worst, spatial resolution (i.e., the ability to distinguish between the intermediate and upwelling zone boxes) is degraded as the result of an overestimate of this parameter. Exchange between the hydrothermal and deep boxes also was estimated and suffers from similar uncertainty. A high value for the exchange flux (40 Sv) was chosen because diapycnal diffusivity increases dramatically near the seafloor, especially near midoceanic ridges, where hydrothermal systems occur (3). Here again, an overestimate of this flux at worst would render the hydrothermal box indistinguishable from the much larger deep ocean box and result in a degradation of spatial resolution.

Major Element Ocean Chemistry. Speciation of S and Fe, mineral saturation states, and some reaction rates require knowledge of the ocean's pH. In addition, some mineral saturation states require knowledge of the concentration of Ca^{2+}. Both these quantities depend on the partial pressure of CO_2 (pCO_2) and on the budgets of major ions in seawater and are estimated in the model as follows. The pCO_2 is taken to be 0.01 atm, consistent with higher greenhouse gas concentrations required for maintaining a warm climate in the face of a weaker middle to late Archean sun (4). Charge balance in the ocean is described by

$$[H^+] - [OH^-] - [HCO_3^-] - 2[CO_3^{2-}] + A + 2[Ca^{2+}] = 0,$$

where A is the non-Ca alkalinity in the ocean (the sum of the charges of the conservative ions other than Ca^{2+}). The Ca^{2+} concentration is limited by $CaCO_3$ saturation, and the concentrations of the inorganic C species depend on pCO_2 and on pH. Expressing these dependences yields

$$[H^+] - \frac{K_W}{[H^+]} - \frac{pCO_2 K_H K_{A1}}{[H^+]} - 2\frac{pCO_2 K_H K_{A1} K_{A2}}{[H^+]^2} + A + 2\frac{K_{SP}[H^+]^2}{pCO_2 K_H K_{A1} K_{A2}} = 0.$$

This quartic equation for $[H^+]$ has only one real, positive root. Solving it yields the pH. The Ca^{2+} concentration then is simply

$$[Ca^{2+}] = \frac{K_{SP}[H^+]^2}{pCO_2 K_H K_{A1} K_{A2}}.$$

In both these equations, K_H is the Henry's law constant for CO_2, K_{A1} and K_{A2} are the first and second acid dissociation constants, K_{SP} is the solubility product constant for calcite, and K_W is the water dissociation constant (Table S3).

Starting with preindustrial values for pCO_2, total alkalinity ($A + 2[Ca^{2+}]$) and the average degree of calcite supersaturation in the ocean (280 μatm, 2.35 mEq and 4, respectively), it is possible to solve for the modern value of A. Making the simplifying assumption that the effect of changing pCO_2 on the total charge of conservative ions in the ocean is exclusively through its effect on Ca^{2+} concentrations, it is possible to solve the equation for $[H^+]$ using the modern value of A and arbitrary pCO_2. For pCO_2 of 0.01 atm and at the temperature of the surface ocean (taken as 15 °C), the following values are obtained: pH = 7.34, [A] = 9.48 mEq, and $[Ca^{2+}]$ = 10.8 mM. These values are assumed to hold in the entire ocean.

Exchange with Sediments. Exchange between sediments and overlying seawater was estimated from a simple model, as follows. A simplified mass balance of S and Fe species in the sediment is

$$\frac{d}{dt}S^{ox}_{pw} = J_w\left(S^{ox}_{sw} - S^{ox}_{pw}\right) - k_{BSR}S^{ox}_{pw},$$

$$\frac{d}{dt}S^{0}_{pw} = J_{S^0} - k_{BSR}S^{0}_{pw},$$

$$\frac{d}{dt}S^{II-}_{pw} = J_w\left(S^{II-}_{sw} - S^{II-}_{pw}\right) + k_{BSR}S^{ox}_{pw} + k_{BSR}S^{0}_{pw} - 2\times J_{py},$$

$$\frac{d}{dt}Fe^{III}_{pw} = J_{Fe^{III}} - k_{BFeR}Fe^{III}_{pw},$$

$$\frac{d}{dt}Fe^{II}_{pw} = J_w\left(Fe^{II}_{sw} - Fe^{II}_{pw}\right) + k_{BFeR}Fe^{III}_{pw} - J_{py}.$$

S^{ox}, S^0, and S^{II-} are total sulfoxy anions, elemental S, and sulfide, respectively. Fe^{II} and Fe^{III} are ferrous and ferric iron, respectively. The subscripts *sw* and *pw* denote seawater and porewater, respectively. J_w is the equivalent of a flux of water between the water column and sediments, used to represent seawater–sediment exchange. k_{BSR} and k_{BFeR} are the rates of sulfur species and Fe^{3+} reduction, respectively, both taken to be 4.6×10^{-9} s^{-1} (*SI Materials and Methods, Biological Activity*). J_{S^0}, $J_{Fe^{III}}$, and J_{py} are the deposition fluxes of S_8 particles, Fe^{3+} particles, and the precipitation flux of sedimentary pyrite, respectively.

Assuming steady state and pyrite precursor saturation ($Fe^{II}_{pw} = K^*_{FeS}/S^{II-}_{pw}$), the equations may be rearranged to give this quadratic equation for S^{II-}_{pw}:

$$-\frac{1}{2}J_W S^{II-2}_{pw} + \left[\frac{1}{2}\left(J_W + \frac{k_{BSR}J_w S^{ox}_{sw}}{k_{BSR} + J_w} + J_{S^0}\right) - \left(J_w Fe^{II}_{sw} + J_{Fe^{III}}\right)\right]S^{II-}_{pw} + J_w K^*_{FeS} = 0,$$

where $K^*_{FeS} = K_{FeS} \times [H^+]^2$. Given values for J_W, S^{ox}_{sw}, Fe^{II}_{sw}, J_{S^0}, $J_{Fe^{III}}$, and ocean pH, this equation may be solved for the value of S^{II-}_{pw} and the fluxes of S to pyrite and back to the water column

may be calculated. In the present day, a flux of sulfide from the sediments to the ocean gets oxidized within the upper oxic sediments or within the water column, whereas in the Precambrian, such a flux would be another source term contributing to the sulfide mass balance in seawater.

Constraints from the present day and the Precambrian may be used to estimate the value of J_w. Today, $S^{ox}_{sw} = [SO_4^{2-}] = 28$ mM, $Fe^{II}_{sw} = [Fe^{2+}] \sim 0$, $J_{S^0} = 0$, and $J_{Fe^{III}} \sim 10^{13}$ mol Fe per year according to estimates of the amount of reactive Fe reaching the oceans (5), and the pH of the ocean is 8.2. In the Archean ocean, $S^{ox}_{sw} \sim 0.2$ mM, $Fe^{II}_{sw} \sim 1$ μM, J_{S^0} can be estimated from photochemical models to be ~10% of the fluxes of S to the ocean, and $J_{Fe^{III}}$ is estimated to be 1/10 the present-day flux as the result of less oxidative weathering of Fe-bearing minerals. The pH of the Archean ocean is estimated to be ~7.3 (*SI Materials and Methods, Major Element Ocean Chemistry*). With these values of the parameters, a value of J_w must be chosen to meet constraints from the S isotope record. In today's ocean sediments, it is estimated that 75–90% of the sulfide produced by sulfate reduction becomes reoxidized (6, 7). Thus, only 10–25% of the S forms pyrite at "first pass." With $J_w = 3 \times 10^{15}$ L per year, ~24% of the S forms first-pass pyrite and the rest becomes oxidized. With the Archean values of the parameters, this value of J_w leads to 92% formation of first-pass pyrite, consistent with ideas that essentially all S exited the ocean as pyrite (8) and with observations of strong radial isotopic gradients in pyrite nodules, which indicate Rayleigh distillation of S isotopes during quantitative reduction of S species to form sulfide, coupled to formation of pyrite (9).

Hydrothermal Systems. The volume of water entering (and exiting) axial hydrothermal systems was taken from ref. 10. The chemistry of the water entering the hydrothermal systems was taken to be identical to model seawater chemistry. Anhydrite, which commonly forms in present-day hydrothermal systems as seawater heats up to ~100 °C, remains undersaturated at the Ca^{2+} and SO_4^{2-} concentrations reached in the model.

It is assumed that all S species are thermally reduced to sulfide during water–rock interactions with Fe^{2+}-bearing minerals in the ocean crust. Some of the sulfide may return to the ocean through hydrothermal vents, depending on the concentrations of Fe and S in hydrothermal fluids as they cool. Estimates of Fe and S concentrations in Archean hydrothermal fluids (11) are added to the concentrations of seawater-derived sulfide and Fe^{2+}. Depending on these total concentrations, either sulfide or Fe^{2+} will be scavenged completely from the cooling fluids by iron sulfide mineral precipitation. The remaining ion (sulfide or Fe^{2+}) will be emitted into the ocean. Because at least some of the S may originally be sourced from seawater species, the weighted average sulfur isotope mass-independent fractionation (S MIF) carried by hydrothermal sulfide fluxes may be nonzero. At the concentrations of S species reached in the model, however, hydrothermal fluids are always a source of Fe^{2+} and not of sulfide, which precipitates within the hydrothermal systems. It still is possible that this sulfide, which does not enter the ocean, carries S MIF, which is preserved in the subseafloor portion of hydrothermal systems.

Chemical Reactions. Chemical equilibria are in Table S3. Nonequilibrium aqueous-phase reactions are in Table S4.

Biological Activity. Microbial reduction of sulfoxy anions, S_8, and Fe^{3+} particles is taken to occur within the sediment. Compiled data on environment-dependent rates of microbial sulfate reduction (12) were used to calculate area-weighted average rates for shallow- and deep-water sediments (0.096 and 0.001 mmol SO_4^{2-} per centimeter^{-2} per year, respectively). Using these values together with the fractional area of shallow and deep environments from paleogeographic reconstructions (13), a global average rate was calculated through Phanerozoic time. The global average rate varies between a modern value of ~0.01 and Paleozoic values as high as ~0.04 mmol SO_4^{2-} per centimeter^{-2} per year. With present-day seawater sulfate concentrations and seafloor area, the higher rates translate into a global rate constant of $\sim 4.6 \times 10^{-9}$ s^{-1}. This rate constant was used for all the S species and for Fe^{3+}. The rates of microbial reduction of various S species and Fe^{3+} likely differ somewhat from this value, but the uncertainty introduced by this choice is acceptable given the other uncertainties associated with the model. A reoxidation rate of the sulfide to elemental S, presumably by Fe^{3+} particles, was taken to be 10^{-6} the reduction rate. The results are insensitive to this choice. An assumption inherent in this approach to estimating the microbial reduction rate constant is that organic carbon delivery to Archean sediments is comparable with modern delivery. This is a reasonable assumption despite suggestions of lower primary productivity, because the scarcity of electron acceptors in the Archean ocean implies less respiration of organic matter within the water column and similar rates of organic matter delivery to the sediments.

The reduced species produced in the sediment (sulfide and Fe^{2+}) may diffuse back into seawater, reoxidize (to S^0 and Fe^{3+}), or be scavenged by formation of iron sulfide minerals. As formation of FeS precursors to pyrite is rapid (14), little sulfide diffuses back to the ocean in the model.

Fraction of S_8 from Photodissociation vs. Photoexcitation. As mentioned in the main text and *Materials and Methods*, S_8 may form from dissociation of SO_2 to form SO, S, and ultimately S_8, or from the reaction of photoexcited SO_2 with other molecules, leading to loss of the oxygen from SO_2. The rate constant for production of S_8 by each of these pathways depends on the absorption cross-section of SO_2 (σ), the incident radiation at the relevant wavelengths (I), and the quantum yield of the pathway (Y):

$$J = \int \sigma(\lambda) I(\lambda) Y(\lambda) d\lambda.$$

The fraction of S_8 formed from photoexcited SO_2, $f^*_{S_8}$, is simply $J_{exc}/(J_{exc} + J_{dis})$, where the subscripts *dis* and *exc* denote integration over the spectral regions in which SO_2 photodissociates (170–220 nm) or becomes photoexcited [260–340 nm (15)]. The yield of the photodissociation reaction is greater than 90% (taken to be 90% in the calculations below), whereas the photoexcitation results in reaction (rather than quenching) only ~10% of the time (15). Reaction of photoexcited SO_2 with a second molecule to form SO occurs only for a limited list of molecules (e.g., ground-state SO_2, CO). To account for this, the quantum yield of this pathway is taken to be 0.1%. With these values, and with SO_2 absorption cross-section data (16) and solar flux data (Fig. S1), a value of $f^*_{S_8}$ of 0.006 is obtained. That is, less than 1% of the S_8 produced in the atmosphere comes from reaction of photoexcited SO_2, with the rest (>99%) coming from direct SO_2 photolysis.

This approach approximates the solar flux incident on SO_2 in the troposphere as identical to the present-day solar spectrum, unmodified by absorption or scattering due to other gases or particles in the Archean atmosphere. Although it is widely appreciated that the sun's early spectrum likely differed from that of today, in the spectral region of interest (~180–360 nm), the flux incident at or near the surface was approximately uniformly weaker (17). The relative (not absolute) rate constant for photolysis over a certain spectral interval therefore is insensitive to secular variation in the sun's luminosity. Additionally, the composition of the ancient atmosphere is unknown. Making a choice about attenuation of the incident solar spectrum by gases other than N_2, H_2O, and CO_2 seems unwarranted. Even so, the uncertainty incurred by attenuation of the solar flux by other atmospheric constituents on calculation of the relative rate constant is small compared with other model uncertainty, unless attenuation is heavily weighted to either

the photodissociation or photoexcitation bands of SO_2. As such, the result that most S_8 (>95%) is generated from SO_2 dissociation, not excitation, is unlikely to change.

Evaporite Formation and Burial. Despite low sulfate levels in the Archean ocean, evaporation of seawater from shallow restricted basins in latitudes of net evaporation inevitably led to supersaturation and deposition of salts, including sulfate minerals. Defining the amount of water evaporated from the ocean in evaporative events sufficient to cause precipitation of sulfate evaporites as "effective evaporation," the burial rate of sulfate evaporite, J_e, is then

$$J_e = J_{EE}\left[SO_4^{2-}\right],$$

where J_{EE} is the effective evaporation of seawater in liters per year. The value of J_{EE} can be estimated from the Phanerozoic records of sulfate evaporite burial and seawater sulfate concentrations (18, 19) by rearranging the above equation to solve for J_{EE}. Doing this, a value of 3.3×10^{13} L per year is obtained. This value of effective evaporation was multiplied by the sulfate concentration of the continental shelf box to dynamically calculate the rate of sulfate evaporite deposition and burial in the model.

1. Hotinski RM, Kump LR, Najjar RG (2000) Opening Pandora's Box: The impact of open system modeling on interpretations of anoxia. *Paleoceanogr* 15:267–279.
2. Huthnance JM, Holt JT, Wakelin SL (2009) Deep ocean exchange with west-European shelf seas. *Ocean Sci* 5:621–634.
3. Kunze E, Firing E, Hummon JM, Chereskin TK, Thurnherr AM (2006) Global abyssal mixing inferred from lowered ADCP shear and CTD strain profiles. *J Phys Oceanogr* 36:1553–1576.
4. von Paris P, et al. (2008) Warming the early earth—CO_2 reconsidered. *Planet Space Sci* 56:1244–1259.
5. Poulton SW, Raiswell R (2002) The low-temperature geochemical cycle of iron: From continental fluxes to marine sediment deposition. *Am J Sci* 302:774–805.
6. Jorgensen BB (1982) Mineralization of organic matter in the sea bed—the role of sulphate reduction. *Nature* 296:643–645.
7. Canfield DE (1991) Sulfate reduction in deep-sea sediments. *Am J Sci* 291(2):177–188.
8. Canfield DE (2004) The evolution of the Earth surface sulfur reservoir. *Am J Sci* 304: 839–861.
9. Fischer WW, et al. (2011) A dynamic Archean sulfur cycle. *Mineral Mag* 75:850 (abstr).
10. Elderfield H, Schultz A (1996) Mid-ocean ridge hydrothermal fluxes and the chemical composition of the ocean. *Annu Rev Earth Planet Sci* 24:191–224.
11. Kump LR, Seyfried WE (2005) Hydrothermal Fe fluxes during the Precambrian: Effect of low oceanic sulfate concentrations and low hydrostatic pressure on the composition of black smokers. *Earth Planet Sci Lett* 235:654–662.
12. Canfield DE, Thamdrup B, Kristensen E (2004) *Aquatic Geomicrobiology. Advances in Marine Biology* (Elsevier, Amsterdam), Vol 48.
13. Halevy I, Peters SE, Fischer WW (2012) Sulfate burial constraints on the Phanerozoic sulfur cycle. *Science* 337(6092):331–334.
14. Rickard D, Luther GW, 3rd (2007) Chemistry of iron sulfides. *Chem Rev* 107(2): 514–562.
15. Okabe H (1978) *Photochemistry of Small Molecules* (Wiley, New York).
16. Keller-Rudek H, Moortgat GK (2009) MPI-Mainz UV-VIS spectral atlas of gaseous molecules. Available at www.atmosphere.mpg.de/spectral-atlas-mainz. Accessed September 1, 2012.
17. Claire MW, et al. (2012) The evolution of solar flux from 0.1 nm to 160 mm: Quantitative estimates for planetary studies. *Astrophys J* 12:95–106.
18. Halevy I, Peters SE, Fischer WW (2012) Sulfate burial constraints on the Phanerozoic sulfur cycle. *Science* 337(6092):331–334.
19. Horita J, Zimmermann H, Holland HD (2002) Chemical evolution of seawater during the Phanerozoic. *Geochim Cosmochim Acta* 66:3733–3756.

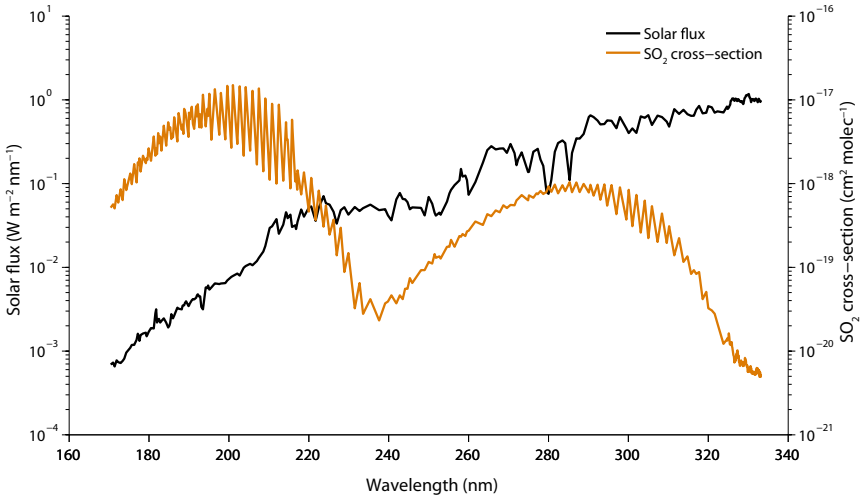

Fig. S1. Solar influx (black) and SO_2 absorption cross-section (orange) over the spectral region in which SO_2 photodissociates (~170–220 nm) and photoexcites (~260–340 nm). Convolving these spectra, multiplying by the quantum yield, and integrating over a spectral interval of interest give the photolysis rate constant in that interval. The ratio of the photolysis rate constant in the photoexcitation region to the total photolysis rate constant gives the value of $f_{S8}^{\natural}$ used in the model (0.006).

Table S1. Geometric and physical properties of the model boxes and prescribed chemical concentrations

Box no.	Ocean box	Surface area, km^2	Volume, km^3	T, °C	$[O_2]$, nM*	$[CH_2O]$, μM
1	Surface	3.1×10^8	3.3×10^7	15	0.33	1.0
2	Intermediate	—	3.4×10^8	10	0.00	0.0
3	Deep	—	1.3×10^9	5	0.00	0.0
4	Deep sediments	—	1.8×10^5	5	0.00	0.0
5	High-lat. downwelling	2.9×10^7	2.9×10^7	5	0.39	1.0
6	High-lat. upwelling	2.9×10^7	2.9×10^7	5	0.39	1.0
7	Continental shelf	3.8×10^7	3.8×10^6	20	0.30	1.0
8	Continental shelf sediments	—	1.9×10^4	20	0.00	0.0
9	Estuaries	7.6×10^6	7.6×10^5	20	0.30	1.0
10	Estuarine sediments	—	3.8×10^3	20	0.00	0.0
11	Near-hydrothermal	—	3.9×10^6	5	0.00	0.0
12	Near-hydrothermal sediments	—	8.6×10^3	5	0.00	0.0
13	Upwelling zones	1.9×10^7	1.1×10^6	10	0.36	0.2
14	Upwelling zone sediments	—	9.5×10^3	10	0.00	0.0

High-latitude boxes were taken to extend northward and southward of ±60°. The surface, intermediate, and deep boxes extend between ±60°. The surface ocean box extends vertically from the surface to a depth of 100 m, the intermediate box between 100 and 1,000 m, and the deep box from 1,000 to 4,000 m. The vertical extent of the high-latitude boxes is from the surface to a depth of 1,000 m. The dissolved O_2 concentration in ocean boxes in contact with the atmosphere was taken to be in equilibrium with the atmospheric concentration of O_2. In subsea surface boxes, the concentration of dissolved O_2 was taken to be zero. Formaldehyde concentrations were estimated based on photochemical models (1), and used to calculate the concentration of sulfite complexed as $CH_2OHSO_3^-$.

*Atmospheric O_2 levels were taken to be 10^{-8} present atmospheric levels.

1. Pinto JP, Gladstone GR, Yung YL (1980) Photochemical production of formaldehyde in Earth's primitive atmosphere. *Science* 210(4466):183–185.

Table S2. Material fluxes among the model boxes

Material flux	Flux magnitude, Sv	Source
Diffuse exchange		
Surface ↔		
Intermediate	60	(1)
Continental	20	Ref. 2 and *SI Materials and Methods*
Intermediate ↔		
Deep	38	(3)
Continental	10	Ref. 2 and *SI Materials and Methods*
Upwelling	10	*SI Materials and Methods*
Deep ↔		
UHL	48	(3)
Hydrothermal	40	*SI Materials and Methods*
Directional flow		
Intermediate → DHL*	19	(3)
DHL → Deep*	19	(3)
Deep → UHL*	19	(3)
UHL → Intermediate*	19	(3)
Surface → Intermediate†	0.40	(4)
Intermediate → Upwelling†	0.40	(4)
Upwelling → Surface†	0.40	(4)
Rivers → Estuaries‡	1.25	(5)
Estuaries → Continental‡	1.25	(5)
Continental → Surface‡	1.25	(5)
Surface → Atmosphere‡	1.25	(5)
Exchange with sediments		
Continental ↔ Continental seds.	9.1×10^{-4}	*SI Materials and Methods*
Estuaries ↔ Estuarine seds.	1.8×10^{-4}	*SI Materials and Methods*
Deep ↔ Deep seds.	8.5×10^{-3}	*SI Materials and Methods*
Hydrothermal ↔ Hydrothermal seds.	4.5×10^{-4}	*SI Materials and Methods*
Upwelling ↔ Upwelling seds.	4.5×10^{-4}	*SI Materials and Methods*
Hydrothermal circulation, near-axis	9.5×10^{-4}	(5)
Effective evaporation, continental shelf	1.0×10^{-3}	*SI Materials and Methods*

See *SI Materials and Methods, Model Geometry and Transport* for details. DHL, downwelling high latitude; UHL, upwelling high latitude.
*Thermohaline circulation.
†Coastal upwelling.
‡Riverine influx and evaporative outflux.

1. Ganachaud A, Wunsch C (2000) Improved estimates of global ocean circulation, heat transport and mixing from hydrographic data. *Nature* 408(6811):453–457.
2. Huthnance JM, Holt JT, Wakelin SL (2009) Deep ocean exchange with west-European shelf seas. *Ocean Sci* 5:621–634.
3. Hotinski RM, Kump LR, Najjar RG (2000) Opening Pandora's Box: The impact of open system modeling on interpretations of anoxia. *Paleoceanogr* 15:267–279.
4. Rykaczewski RR, Checkley DM, Jr. (2008) Influence of ocean winds on the pelagic ecosystem in upwelling regions. *Proc Natl Acad Sci USA* 105(6):1965–1970.
5. Elderfield H, Schultz A (1996) Mid-ocean ridge hydrothermal fluxes and the chemical composition of the ocean. *Annu Rev Earth Planet Sci* 24:191–224.

Table S3. Aqueous equilibria in the model and their equilibrium constants ($-\log_{10}$) at a temperature of 25 °C, an ionic strength of 0.7, and a salinity of 35 PSU (where relevant)

Reaction	pK*	Ref(s).
$H_2O \rightleftharpoons H^+ + OH^-$	13.63	(1)
$CO_{2(g)} \rightleftharpoons CO_{2(aq)}$	1.55	(2)
$CO_{2(aq)} \rightleftharpoons HCO_3^- + H^+$	5.86	(2)
$HCO_3^- \rightleftharpoons CO_3^{2-} + H^+$	8.92	(2)
$Fe^{2+} + H_2O \rightleftharpoons FeOH^+ + H^+$	9.8	(3)
$Fe^{2+} + 2H_2O \rightleftharpoons Fe(OH)_2 + 2H^+$	20.9	(3)
$Fe^{2+} + 3H_2O \rightleftharpoons Fe(OH)_3^- + 3H^+$	31.1	(3)
$Fe^{3+} + H_2O \rightleftharpoons FeOH^{2+} + H^+$	2.62	(4)
$Fe^{3+} + 2H_2O \rightleftharpoons Fe(OH)_2^+ + 2H^+$	6.79	(4)
$Fe^{3+} + 3H_2O \rightleftharpoons Fe(OH)_3 + 3H^+$	13.62	(4)
$Fe^{3+} + 4H_2O \rightleftharpoons Fe(OH)_4^- + 4H^+$	22.7	(4)
$Fe^{3+} + Cl^- \rightleftharpoons FeCl^{2+}$	−0.57	(4)
$Fe^{3+} + 2Cl^- \rightleftharpoons FeCl^+$	0.13	(4)
$Fe^{3+} + SO_4^{2-} \rightleftharpoons FeSO_4^+$	−2.58	(4)
$Fe^{3+} + 2SO_4^{2-} \rightleftharpoons Fe(SO_4)_2^-$	−3.40	(4)
$SO_{2(aq)} \rightleftharpoons HSO_3^- + H^+$	1.77	(5)
$HSO_3^- \rightleftharpoons SO_3^{2-} + H^+$	7.22	(5)
$2SO_3^{2-} + 2H^+ \rightleftharpoons S_2O_52- + H_2O$	−15.87	(6)
$HSO_3^- + CH_2(OH)_2 \rightleftharpoons CH_2OHSO_3^-$	−5	(7)
$H_2S(aq) \rightleftharpoons HS^- + H^+$	6.51	(8)
$Fe^{2+} + HS^- \rightleftharpoons FeHS^+$	−5.3	(8)
$Fe^{2+} + HS^- \rightleftharpoons FeS + H^+$	2.2	(8)
$HS^- + {}^{(n-1)}/_8 S_{8(s)} \rightleftharpoons S_n^{2-} + H^+$	†	(9)
$HS^- + {}^{(n-1)}/_8 S_{8(s)} \rightleftharpoons HS_n^-$	‡	(9)
$H^+ + HS^- + {}^{(n-1)}/_8 S_{8(s)} \rightleftharpoons H_2S_n$	§	(9)
$3H^+ + Fe(OH)_{3(s)} \rightleftharpoons Fe^{3+} + 3H_2O$	−4.5	(4)
$FeCO_{3(s)} \rightleftharpoons Fe^{2+} + CO_3^{2-}$	10.52	(10)
$H^+ + FeS_{(s)} \rightleftharpoons Fe^{2+} + HS^-$	3.5	(8)
$CaSO_{4(s)} \rightleftharpoons Ca^{2+} + SO_4^{2-}$	5.39	(11)
$CaCO_{3(s)} \rightleftharpoons Ca^{2+} + CO_3^{2-}$	6.37	(2)

PSU, practical salinity units.

*At 25 °C, I = 0.7, S = 35.

†n = (2–8), pK = [11.46, 10.44, 9.70, 9.47, 9.66, 10.24, 10.79].

‡n = (2–8), pK = [1.76, 2.94, 3.40, 3.76, 4.43, 5.33, 6.11].

§n = (2–8), pK = [–3.24, –1.26, –0.40, 0.26, 1.07, 2.08, 2.95].

1. Millero FJ, Sotolongo S, Izaguirre M (1987) The oxidation kinetics of Fe(II) in seawater. *Geochim Cosmochim Acta* 51:793–801.
2. Zeebe RE, Wolf-Gladrow DA (2001) *CO_2 in Seawater: Equilibrium, Kinetics, Isotopes* (Elsevier, Amsterdam).
3. Millero FJ, Sotolongo S (1989) The oxidation of Fe(II) by H_2O_2 in seawater. *Geochim Cosmochim Acta* 53:1867–1873.
4. Millero FJ, Yao WS, Aicher J (1995) The speciation of Fe(II) and Fe(III) in natural waters. *Mar Chem* 50:21–39.
5. Jacobson MZ (2005) *Fundamentals of Atmospheric Modeling* (Cambridge Univ Press, New York) 2nd Ed.
6. Minteq thermodynamic database. Available at www2.lwr.kth.se/English/OurSoftware/vminteq. Accessed September 1, 2012.
7. Chameides WL (1984) The photochemistry of a remote marine stratiform cloud. *J Geophys Res-Atm* 89:4739–4755.
8. Rickard D, Luther GW, 3rd (2007) Chemistry of iron sulfides. *Chem Rev* 107(2):514–562.
9. Kamyshny AJ, Jr., Goifman A, Gun J, Rizkov D, Lev O (2004) Equilibrium distribution of polysulfide ions in aqueous solutions at 25 ° C: A new approach for the study of polysulfides' equilibria. *Environ Sci Technol* 38(24):6633–6644.
10. Benezeth P, Dandurand JL, Harrichoury JC (2009) Solubility product of siderite ($FeCO_3$) as a function of temperature (25–250 °C). *Chem Geol* 265:3–12.
11. Lide DR (2006) *CRC Handbook of Chemistry and Physics* (CRC, Boca Raton, FL), 87th Ed.

Table S4. Nonequilibrium aqueous reactions in the model and expressions for their rates

Reaction	Rate, $M \cdot s^{-1}$	Ref(s).
$SO_3^{2-} + ½O_2 \rightarrow SO_4^{2-}$	$0.103\alpha HSO_3^- \alpha SO_3^{2-}[O_2]^{½}[S^{IV}]$	(1)
$SO_3^{2-} + 2Fe^{3+} \rightarrow SO_4^{2-} + 2Fe^{2+}$	$(77.5\alpha FeOH^{2+} + 20.22\alpha Fe(OH)_2^+)\alpha HSO_3^-[Fe^{III}][S^{IV}]$	(2)
$SO_3^{2-} + H_2O_2 \rightarrow SO_4^{2-} + H_2O$	$[H^+]/([H^+]+0.1)\exp(-3,650(1/T-1/298))\alpha HSO_3^-[H_2O_2][S^{IV}]$	(3)
$4SO_3^{2-} + H^+ \rightarrow 2SO_4^{2-} + S_2O_3^{2-} + H_2O$	$\exp(-Ea/RT)(\alpha SO_2(aq) + \alpha HSO_3^- + \alpha SO_3^{2-} + 2\alpha S_2O_5^{2-})[S^{IV}]$*	(4–6)
$S_3O_6^{2-} + H_2O \rightarrow S_2O_3^{2-} + SO_4^{2-} + 2H^+$	$1.125\times10^9\exp(-Ea/RT)\alpha S_3O_6^{2-}[S_nO_6^{2-}]$†	(7, 8)
$S_4O_6^{2-} + SO_3^{2-} \rightarrow S_3O_6^{2-} + S_2O_3^{2-}$	$0.55^-\alpha SO_3^{2-}\alpha S_4O_6^{2-}[S^{IV}][S_nO_6^{2-}]$	(9)
$S_4O_6^{2-} + S_2O_3^{2-} \leftrightarrow S_5O_6^{2-} + SO_3^{2-}$	*forward* $2.12\times10^{-4}\alpha S_4O_6^{2-}[S_2O_3^{2-}][S_nO_6^{2-}]$	(8)
	backward $1,000\alpha SO_3^{2-}\alpha S_5O_6^{2-}[S^{IV}][S_nO_6^{2-}]$	(9)
$S_5O_6^{2-} + S_2O_3^{2-} \leftrightarrow S_6O_6^{2-} + SO_3^{2-}$	*forward* $0.95\times10^{-4}\alpha S_5O_6^{2-}[S_2O_3^{2-}][S_nO_6^{2-}]$	(8)
	backward $\alpha SO_3^{2-}\alpha S_6O_6^{2-}[S^{IV}][S_nO_6^{2-}]$	Est
$S_5O_6^{2-} + 3OH^- \rightarrow 2½S_2O_3^{2-} + 1½H_2O$	$0.513\alpha S_5O_6^{2-}[OH^-][S_nO_6^{2-}]$	(10)
$S_2O_3^{2-} + 2H_2O_2 \rightarrow 2SO_3^{2-} + 3H^+ + H_2O$	$0.025[H_2O_2][S_2O_3^{2-}](1-f_{PT})$‡	(9)
$S_2O_3^{2-} + H_2O_2 \rightarrow S_4O_6^{2-} + 2OH^-$	$0.025[H_2O_2][S_2O_3^{2-}]f_{PT}$	(9)
$S_2O_3^{2-} + H^+ \rightarrow SO_3^{2-} + ⅛S_8 + H^+$	$1.64\times10^{11}\exp(-Ea/RT)[H^+][S_2O_3^{2-}]$§	(11)
$H_2S + 1½O_2 \rightarrow SO_3^{2-} + 2H^+$	$\left(10\text{^}\left(10.50+0.16pH-3000/T+0.44I^{½}\right)\right)\Big/3600(\alpha H_2S+\alpha HS^-)[O_2][S^{II-}]$	(12)
$H_2S + SO_3^{2-} + ½O_2 \rightarrow S_2O_3^{2-} + H_2O$	$\exp(28.92+0.0369S-0.8032.68/T)/60\alpha SO_3^{2-}(\alpha H_2S+\alpha HS^-)[S^{IV}][S^{II-}]$	(13)
$H_2S + H_2O_2 \rightarrow ⅛S_8 + 2H_2O$	$\exp(25-6306/T)/60\alpha H_2S[H_2O_2]\ \ [S^{II-}]$	(14)
$H_2S + h\nu \rightarrow ⅛S_8 + H_2$	$0.04/60/4(\alpha H_2S+\alpha HS^-)[S^{II-}]$¶	(15)
$2Fe^{2+} + ½O_2 + H_2O \rightarrow 2Fe^{3+} + 2OH^-$	$\left(10\text{^}(21.56-1545/T-3.29I^{½}+1.52I)\right)\Big/60[OH]^2[O_2][Fe^{II}]$	(16)
$2Fe^{2+} + H_2O_2 \rightarrow 2Fe^{3+} + 2OH^-$	$\left(10\text{^}(8.37-1866/T)\alpha Fe^{2+} + 10\text{^}(17.26-2948/T-1.70I^{½}+1.20I)\alpha FeOH^+\right)[H_2O_2][Fe^{II}]$	(17)
$2Fe^{2+} + 2H^+ + h\nu \rightarrow 2Fe^{3+} + H_2$	$1.1\times10^{-7}[Fe^{II}]$‖	(18)

Est, estimated.

*Ea = 40 or 50 $kJ \cdot mol^{-1}$ (sensitivity to this value is included in the range of concentrations in Fig. 3). R is the gas constant.

†Ea = 87.09 $kJ \cdot mol^{-1}$.

‡f_{PT} is the fraction of reaction products that end up as polythionates. From a fit to the data in ref. 9:
$f_{PT} = \frac{0.8}{1+e^{2(pH-7)}}$.

§Ea = 66.70 $kJ \cdot mol^{-1}$.

¶The factor of 1/4 in the rate accounts for photolysis for only 6 h out of the day.

‖Rate constant was calculated on the basis of estimates in ref. 18 of photooxidation of 200 mg Fe centimeters^{-2} per year^{-1} for a modern solar flux hitting a water column with 100 μM Fe^{2+} and reacting down to a depth of 100 m.

1. Zhang JZ, Millero FJ (1991) The rate of sulfite oxidation in seawater. *Geochim Cosmochim Acta* 55:677–685.
2. Millero FJ, Gonzales-Davila M, Santana-Casiano JM (1995) Reduction of Fe(III) by sulfite in natural waters. *J Geophys Res-Atm* 100:7235–7244.
3. Stevenson DS, et al. (2003) Atmospheric impact of the 1783-1784 Laki eruption: Part I chemistry modelling. *Atmos Chem Phys* 3:487–507.
4. Ryabinina AF, Oshman VA (1972) Thermal decomposition of aqueous sulfur dioxide solutions. *Tr Ural Lesotekh Inst* 28:182–189.
5. Rempel SI, Ryabinina AF, Oshman VA (1974) *Kinetics and mechanism of the thermal decomposition of solutions of sulfur dioxide and bisulfites. Ural Lesotekh Inst deposited document*, 31 pp. Russian.
6. Guekezian M, Coichev N, Suarez-Iha MEV, de Almeida-Neves E (1997) Stability of sulfur(IV) solutions in the presence of amines and the tendency of sulfite solution to disproportionate in stock solutions. *Anal Lett* 30:1423–1436.
7. Naito K, Hayata H, Mochizuki M (1975) The reactions of polythionates: Kinetics of the cleavage of trithionate ion in aqueous solutions. *J Inorg Nucl Chem* 37:1453–1457.
8. Zhang H, Jeffrey MI (2010) A kinetic study of rearrangement and degradation reactions of tetrathionate and trithionate in near-neutral solutions. *Inorg Chem* 49(22):10273–10282.
9. Lu Y, Gao Q, Xu L, Zhao Y, Epstein IR (2010) Oxygen-sulfur species distribution and kinetic analysis in the hydrogen peroxide-thiosulfate system. *Inorg Chem* 49(13):6026–6034.
10. Pan C, et al. (2011) Kinetics and mechanism of alkaline decomposition of the pentathionate ion by the simultaneous tracking of different sulfur species by high-performance liquid chromatography. *Inorg Chem* 50(19):9670–9677.
11. Johnston F, McAmish L (1973) A study of the rates of sulfur production in acid thiosulfate solutions using S-35. *J Colloid Interface Sci* 42:112–119.
12. Millero FJ, Hubinger S, Fernandez M, Garnett S (1987) Oxidation of H_2S in seawater as a function of temperature, pH, and ionic strength. *Environ Sci Technol* 21(5):439–443.
13. Zhang JZ, Millero FJ (1993) The products from the oxidation of H_2S in seawater. *Geochim Cosmochim Acta* 57:1705–1718.
14. Yao W, Millero FJ (1996) Oxidation of hydrogen sulfide by hydrous Fe(III) oxides in seawater. *Mar Chem* 52:1–16.
15. Pos WH, Milne PJ, Reimer DD, Zika RG (1997) Photoinduced oxidation of H_2S species: A sink for sulfide in seawater. *J Geophys Res-Oceans* 102:12831–12837.
16. Millero FJ, Sotolongo S, Izaguirre M (1987) The oxidation kinetics of Fe(II) in seawater. *Geochim Cosmochim Acta* 51:793–801.
17. Millero FJ, Sotolongo S (1989) The oxidation of Fe(II) by H_2O_2 in seawater. *Geochim Cosmochim Acta* 53:1867–1873.
18. Braterman PS, Cairns-Smith AG, Sloper RW (1983) Photo-oxidation of hydrated Fe^{2+}—significance for banded iron formations. *Nature* 303:163–164.

Table S5. Model parameter values

Parameter	Value	Source
Surface pressure	1 bar	—
CO_2 partial pressure	0.01 bar	*
O_2 level	10^{-8} present levels	e.g., ref. 1
Earth's radius	6,400 km	
Ocean fraction of surface	0.85	
Volcanic S outgassing	3×10^{11} mol·y^{-1}	(2)
[H_2S] in hydrothermal fluid	20 mM	(3)
[Fe^{2+}] in hydrothermal fluid	80 mM	(3)
Particle settling velocity	100 m·d^{-1}	(4)
Sedimentation rate		
Abyss	1×10^{-5} m·y^{-1}	(5)
Continental shelves	5×10^{-5} m·y^{-1}	(5)
Estuaries	1×10^{-2} m·y^{-1}	(5)
Riverine concentration		
All S species	0 M	†
Fe^{2+}	2.8×10^{-4} m	‡

*Consistent with estimates of the amount of CO_2 required for clement climatic conditions despite lower solar luminosity in the Archean (e.g., ref. 6).
†Assuming that dissolution of pyrite is small and that sulfate evaporites are minor in their contribution to the influx to the ocean relative to volcanic outgassing.
‡Calculated from a riverine influx of 1.25×10^9 L·s^{-1} (7) and estimates of an average value of 1.1×10^{13} mol·y^{-1} of reactive Fe delivered in rivers today (8), assuming that all of the fractions comprising reactive Fe today were dissolved before the rise of O_2.

1. Pavlov AA, Kasting JF (2002) Mass-independent fractionation of sulfur isotopes in Archean sediments: strong evidence for an anoxic Archean atmosphere. *Astrobiology* 2(1):27–41.
2. Halmer MM, Schmincke H-U, Graf H-F (2002) The annual volcanic gas input into the atmosphere, in particular into the stratosphere: a global data set for the past 100 years. *J Volcanol Geotherm Res* 115:511–528.
3. Kump LR, Seyfried WE (2005) Hydrothermal Fe fluxes during the Precambrian: Effect of low oceanic sulfate concentrations and low hydrostatic pressure on the composition of black smokers. *Earth Planet Sci Lett* 235:654–662.
4. McDonnell AMP, Buesseler KO (2010) Variability in the average sinking velocity of marine particles. *Limnol Oceanogr* 55:2085–2096.
5. Eriksson PG, Bose PK, Sarkar S, Banerjee S (2004) *The Precambrian Earth: Tempos and Events*, eds Eriksson PG, Altermann W, Nelson DR, Mueller WU, Catuneanu O (Elsevier, Amsterdam), p 676.
6. von Paris P, et al. (2008) Warming the early earth—CO_2 reconsidered. *Planet Space Sci* 56:1244–1259.
7. Elderfield H, Schultz A (1996) Mid-ocean ridge hydrothermal fluxes and the chemical composition of the ocean. *Annu Rev Earth Planet Sci* 24:191–224.
8. Poulton SW, Raiswell R (2002) The low-temperature geochemical cycle of iron: From continental fluxes to marine sediment deposition. *Am J Sci* 302:774–805.